Ceramics International **23** (1997) 27–37

0272-8842(95)00136-0
0272-8842/97 $17.00+.00

Factors Affecting Mechanical Properties of Silicon Oxynitride Ceramics

Masayoshi Ohashi, Kazuo Nakamura, Kiyoshi Hirao, Motohiro Toriyama & Shuzo Kanzaki

National Industrial Research Institute of Nagoya, Hirate-cho 1-1, Kita-ku, Nagoya 462, Japan

(Received 25 July 1995; accepted 2 September 1995)

Abstract: The effect of additives and impurities on the mechanical properties of silicon oxynitride ceramics was investigated. The toughening of the ceramics was affected by three factors: (1) the thermal tensile stress in the intergranular glassy phase and the compressive stress in Si_2N_2O grains, developed by a thermal expansion mismatch between Si_2N_2O grains and the intergranular glassy phase; (2) the large grain size of Si_2N_2O; and (3) the concentration of impurities in the intergranular glassy phase. The degradation of high-temperature strength was primarily dependent on the basic chemical composition (the kind of additives (MeO_x) and Me/Si ratio) of the intergranular phase and impurities. © 1996 Elsevier Science Limited and Techna S.r.l.

1 INTRODUCTION

Silicon oxynitride (Si_2N_2O) ceramics are considered for use as structural components in high temperatures, as well as silicon nitride (Si_3N_4) and β'-sialon, because of their excellent resistance to oxidation[1–6] and high strength at high temperatures.[4–6] Si_2N_2O ceramics are generally made from Si_3N_4 and SiO_2 powder mixtures with additives. A liquid forms as a result of a reaction between all constituents above a eutectic temperature. The liquid promotes the densification and formation of Si_2N_2O. The volume fraction of the liquid phase decreases as the formation of Si_2N_2O proceeds, such as occurs in the reaction sintering of β'-sialon; however, some liquid remains as intergranular phases.[4–7] The intergranular phases control the properties of Si_2N_2O ceramics.

We are attempting to tailor intergranular phases to control the properties of engineering ceramics with intergranular secondary phases which are formed via liquid-phase sintering. We have also been studying the relation between the properties of intergranular glassy phases and those of bulk bodies for Si_2N_2O ceramics to make the first step in the tailoring of the engineering ceramics. The oxynitride glasses with a variety of chemical compositions have been fabricated and investigated for the estimation of the properties of the intergranular glassy phases at grain boundaries;[8–11] however, the degradation of some properties (strength, oxidation resistance, etc.) at high temperatures may not necessarily be explained on the basis of the properties of the synthesized oxynitride glasses. The intergranular glassy phases (liquid phases) in sintered bodies generally contain impurities which are included in raw powders or contaminated through processings, and the impurities seriously affect the properties of the intergranular glassy phases.

Several researchers[12–18] reported the influence of impurities on high-temperature mechanical properties and densification of silicon nitride ceramics. Ca had significant effects on high-temperature strength and deformation.[12,13,15] Halogens (Cl and F) are also typical impurities in Si_3N_4 raw powders, and degrade the high-temperature properties because of lowering the softening (melting) temperature of the intergranular glassy phases.[14–18] In this study, two kinds of raw Si_3N_4 powders with different impurity contents, especially in fluorine (F) content, were used for investigation into the effect of impurities on the mechanical properties of silicon oxynitride ceramics. Besides, two types of sintering aids (Gd_2O_3 and $Y_2O_3+Al_2O_3$) were

Table 1. Impurity contents in two kinds of Si_3N_4 raw powders (A and B)

ppm	Fe	Al	Ca	Mg	Cl	F	O(%)	C(%)	α/(α+β)	SSA(m^2/g)
A	55	75	20	3	36	1480	1.21	0.16	0.96	22
B	47	11	7	2	25	130	1.24	0.16	0.96	11

α/(α+β): α phase fraction, SSA: specific surface area.

Table 2. Starting compositions of all the Si_2N_2O ceramics investigated

(wt%)	Si_3N_4	SiO_2	Y_2O_3	Al_2O_3	Gd_2O_3	GdF_3
DYA22·UYA22	70·84	22·74	4·46	1·96	—	—
DG15·UG15	71·73	23·02	—	—	5·25	—
UG15F	71·64	23·00	—	—	3·86	1·50

added to equimolar Si_3N_4/SiO_2 powder mixtures because the basic chemical composition of the intergranular phase was also expected to affect the properties of the ceramics. The purpose of this study is to understand the variation in mechanical properties among the several kinds of Si_2N_2O ceramics.

2 EXPERIMENTAL PROCEDURE

Impurity contents in two kinds of starting Si_3N_4 powders (A and B) are summarized in Table 1. Powder (A) contained larger amounts of impurities than powder (B). F, Al and Ca contents in the powder (A) were approximately 11 times, 7 times and 3 times as much as those in the powder (B), respectively. There were no appreciable difference in Fe, Mg, O, C and Cl contents between these powders. Starting oxide powders (SiO_2, Gd_2O_3, Y_2O_3 and Al_2O_3; Hokko Chemical Industry Co. Ltd, Tokyo, Japan) were derived from alkoxides and had a purity of more than 99·9%. GdF_3 (Rare Metallic Co. Ltd, Tokyo, Japan) was also used for investigation into the effect of fluorine on the properties of the bulk bodies or the intergranular phases, and had a purity of 99·9%. The equimolar Si_3N_4/SiO_2 powder was mixed with the metallic oxide and fluoride powders with a vibrational mill for 6 h in methanol using a silicon nitride container and balls. The starting compositions are given in Table 2. DYA22 and DG15 were prepared from the relatively impure Si_3N_4 powder (A), and UYA22, UG15 and UG15F from the relatively pure Si_3N_4 powder (B). The amount of oxygen in the Si_3N_4 powders was counted as another SiO_2 source. In this study, oxygen content of the Si_3N_4 powders was determined to be approximately 1·2 wt%, but they were estimated to be more (4 wt%) by considering the effect of oxidation through processings when the starting compositions were calculated. After drying, the mixed powder was passed through a 60 mesh sieve and then hot-pressed under 29 MPa at 1750°C for 0·5–6 h in 0·1 MPa nitrogen atmosphere. The heating rate was 10°C/min.

Three-point flexural strength was measured at room temperature to 1500°C on bars 3×3×26 mm, ground with a #400 diamond wheel, and chamfered with #600 diamond disk. A span of 20 mm was used with a crosshead speed of 0·5 mm/min. More than 3 bars were used in a measurement at each temperature. Fracture toughness (K_{IC}) was measured by the indentation microfracture (IM) method. It was calculated using the equation by Marshall and Evans.[19] A Vickers indenter was pressed in under a load of 98–196 N. The average values (strength and K_{IC}) of the specimens hot-pressed for 2–6 h were used as the representative values because the variations in strength and K_{IC} were independent of the hot-pressing time within 2–6 h. Young's modulus was measured by an ultrasonic pulse echo method. Bulk density was measured by Archimedes' method, using distilled water. The Young's modulus and the bulk density were used for the calculation of the fracture toughness.

Crystalline phases present were identified by an X-ray diffractometer (XRD) (CuK_α, 40 kV, 100 mA). Microstructures were examined by a scanning electron microscope (SEM). Energy dispersive X-ray spectroscopy (EDS) analysis was conducted on a transmission electron microscope (TEM) in a STEM mode for determination of the chemical composition of the intergranular glasses.

Oxynitride glasses with compositions close to those of the intergranular glasses were synthesized because some physical properties of the intergranular glasses were necessary for the calculation of residual thermal stresses in the ceramics. The fabrication and evaluation method of the oxynitride glasses were described elsewhere.[11]

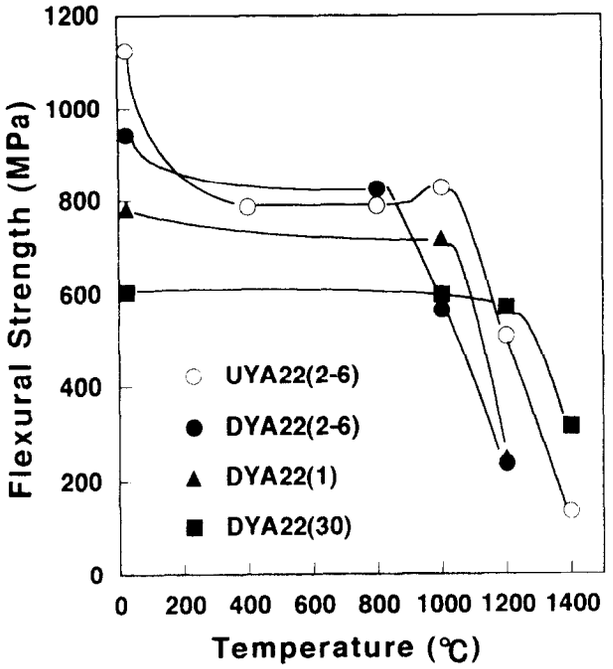

Fig. 1. Temperature dependence of flexural strength of $Y_2O_3 + Al_2O_3$-doped Si_2N_2O ceramics.

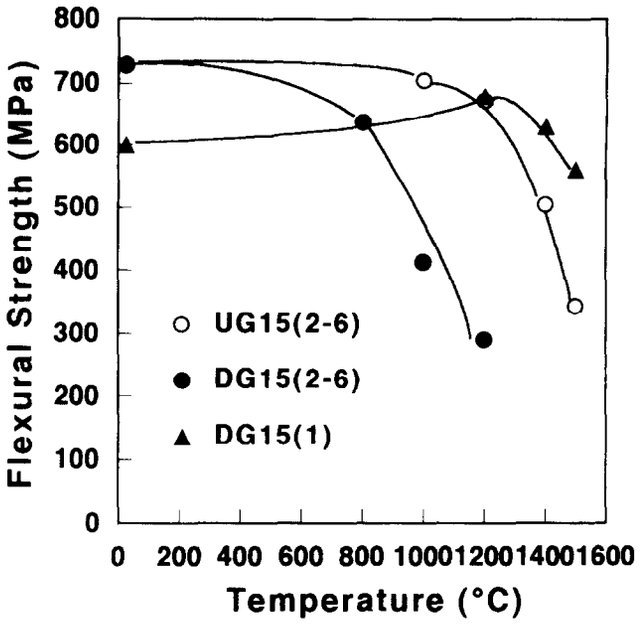

Fig. 2. Temperature dependence of flexural strength of Gd_2O_3-doped Si_2N_2O ceramics.

3 RESULTS

3.1 Flexural strength

Figure 1 shows the temperature dependence of flexural strength of Si_2N_2O ceramics doped with $Y_2O_3 + Al_2O_3$. The hot-pressing time (h) of the sample is designated in parentheses following the sample name, except for the sample hot-pressed for 0·5 h which is referred to as DYA22(30). The strength of DYA22 derived from the powder (A) at room temperature and intermediate temperatures increased with the hot-pressing time, whereas the strength at high temperatures degraded at a lower temperature with the hot-pressing time. In the case of UYA22 derived from the relatively pure powder (B), the strength of the specimens hot-pressed for 2–6 h was very high (> 1 GPa) at room temperature and decreased drastically at an intermediate temperature. However, the strength was maintained until a higher temperature than that of DYA22(2-6). As mentioned above, the average strengths were plotted as the representative values for the specimens hot-pressed for 2–6 h because the variation in strength was independent of the hot-pressing time within 2–6 h.

The flexural strengths of Si_2N_2O ceramics doped with Gd_2O_3 are plotted as a function of temperature in Fig. 2. The strength of DG15 at room temperature increased with the hot-pressing time in a similar manner to that of the ceramics doped with $Y_2O_3 + Al_2O_3$. The strength increased to a maximum at approximately 1200°C, then fell slightly to 1500°C in the Gd_2O_3-doped ones hot-pressed for 1 h (DG15(1)). The strength of the ones hot-pressed for 2–6 h (DG15(2-6)) fell progressively up to 800°C, and sharply at higher temperatures. The use of the pure powder (B) improved the strength at high temperatures. The strength of UG15(2-6) remained almost steady up to 1200°C, and then decreased gradually but still remained relatively high (505 MPa) even at 1400°C, as compared with DG15(2-6).

3.2 Fracture toughness

Figure 3 shows the fracture toughness values of all the Si_2N_2O ceramics in this study, which were measured by the indentation microfracture method. In both cases of the $Y_2O_3 + Al_2O_3$ and Gd_2O_3 additions, the fracture toughness values increased with increasing the hot-pressing time from 0·5 (or 1)–2 h, as shown in Fig. 4. As mentioned above, the average K_{IC} values were used as the representative values for the specimens hot-pressed for 2–6 h because the variations in K_{IC} were independent of the hot-pressing time within 2–6 h. The samples (UYA22(2-6) and UG15(2-6)) prepared from the pure powder (B) had relatively low fracture toughness, as compared to those prepared from the impure powder (A) (DYA22(2-6) and DG15(2-6)). The influence of fluorine on fracture toughness was examined. An intentional addition of 4000 ppm F as GdF_3 (UG15F(6)) made the fracture toughness of UG15(2-6) rise to a level comparable to that of DG15(2-6) prepared from the impure powder.

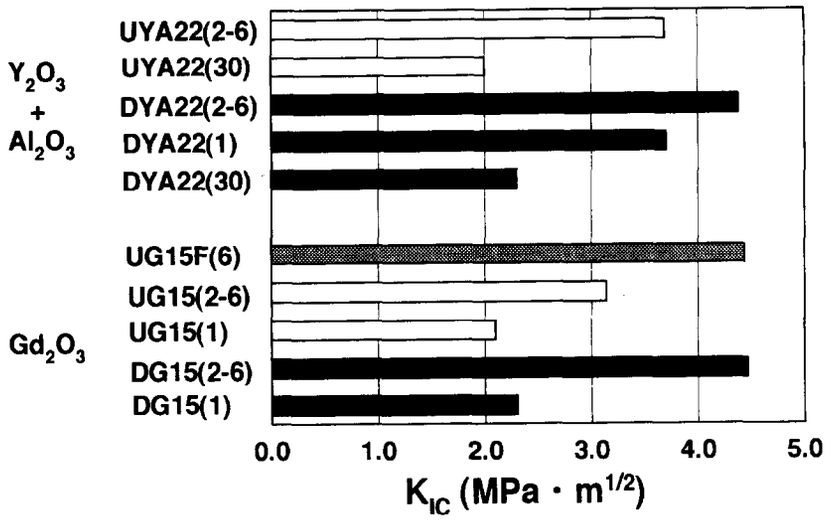

Fig. 3. Fracture toughness values of all the Si_2N_2O ceramics investigated.

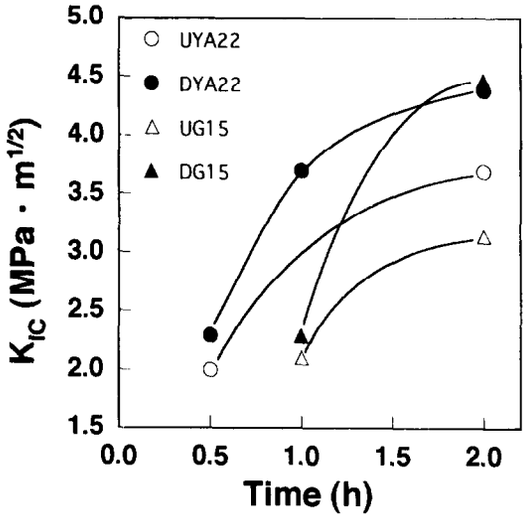

Fig. 4. Variation in fracture toughness of Si_2N_2O ceramics during hot-pressing at 1750°C.

4 DISCUSSION

4.1 Reaction sintering model

Si_2N_2O is formed by the following reaction:

$$Si_3N_4 + SiO_2 \rightarrow 2Si_2N_2O$$

This reaction occurs via a liquid phase which forms as a result of the presence of the metallic oxide additive. Me/Si ratio (where Me = the metallic element of oxides added as sintering aids) of the (intergranular) liquid phase increases as the formation of Si_2N_2O proceeds, because Si_2N_2O is formed through a process whereby Si_3N_4 dissolves and reacts with the SiO_2 component of the intergranular liquid phase, as reported in the previous work[4] (Fig. 5). Si_2N_2O grains grow and the fraction of the intergranular phase reduces as the reaction sintering proceeds.[4–7] Therefore, impurities are concentrated in the intergranular phase progressively. The intergranular liquid phase remains as a glass on cooling until the Me/Si ratio exceeds a certain level, at which point the liquid phase crystallizes at triple grain junctions.[4] With the crystallization, impurities are further concentrated in residual intergranular (glassy) films at two-grain junctions and glassy phases remaining partly at triple grain junctions.

4.2 $Y_2O_3 + Al_2O_3$ addition

Figure 6 shows the microstructures of DYA22 hot-pressed for 0·5–6 h and UYA22 hot-pressed for 2 and 6 h. Elongated Si_2N_2O grains in DYA22 gradually grew with increasing the firing time from 0·5–2 h. Additional grain growth of Si_2N_2O by hot-pressing for periods from 2 to 6 h was observed for neither of the samples (DYA22 and UYA22) as shown in Fig. 7. The Si_2N_2O crystal morphology is that of elongated pseudo-hexagonal prism with the maximum dimension along [001].[20] The average diameters perpendicular to the major prism axis [001] were plotted as the grain sizes along minor axis in Fig. 7. UYA22 prepared from the pure powder had a larger average grain size than DYA22. No crystallization occurred in the intergranular phases of all the samples with Y_2O_3 + Al_2O_3 addition during cooling. The samples hot-pressed for 2 h and more consisted of Si_2N_2O and a small amount of β-Si_3N_4 as crystalline phases identified by XRD. α-Si_3N_4 remained in the sample hot-pressed for 0·5 or 1 h. A larger amount of α-Si_3N_4 was left in the sample hot-pressed for shorter time.

The onset temperature, at which the degradation of strength started to occur, shifted toward lower temperature with increasing the hot-pressing time from 0·5 to 2 h, as shown in Fig. 1. As mentioned

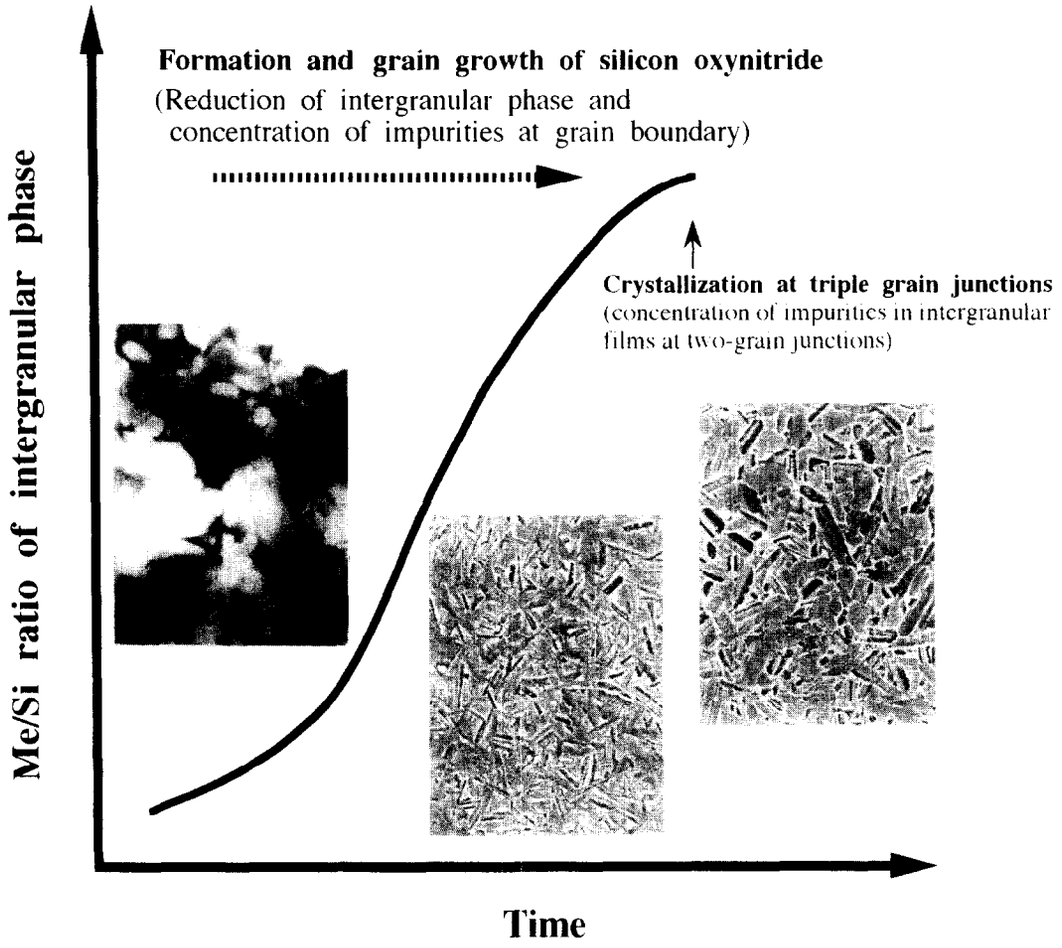

Fig. 5. Diagrammatic summary of the reaction-sintering process of Si_2N_2O ceramics.

above, the reduction of the volume fraction and the change of the chemical composition (i.e. the increase of Me/Si ratio and the concentration of impurities) in the intergranular glassy phase are considered to occur as the reaction sintering proceeds. Chemical analyses were carried out on triple grain junctions using EDS mounted on TEM. Chemical compositions were calculated on the assumption that the intergranular phase was composed of Y, Al, Si and O without any nitrogen atoms, because oxygen and nitrogen could not be measured by the EDS. The average (Y + Al)/Si ratio of the intergranular glassy phases (triple junctions) increased with the hot-pressing time from 0·5 to 2 h, as shown in Table 3. Impurity elements (e.g. Fe, Ca) were not detected. F could not be measured by the EDS used in this study; however, Isozaki *et al.* confirmed the existence of halogens (Cl, F) in the intergranular phase of a Si_3N_4 ceramic. The ceramic was prepared from a powder containing 440 ppm F and 10 ppm Cl, and 310ppm F and 30ppm Cl were determined in the ceramic by a chemical analysis using a higher resolution TEM + EDS system. The powder (A) was prepared by the same method (nitridation of silicon) as that of the powder used in their study and included more amounts of F. Therefore, appreciable amounts of F probably exist in the intergranular phases of DYA22 prepared from powder (A). The high-temperature strength of UYA22(2-6) prepared from the pure powder was higher than that of DYA22(2-6). The results obviously suggest great influence of impurities in the starting Si_3N_4 powder on the viscosity of the intergranular glass at high temperatures. The shift of the onset temperature with the hot-pressing time for DYA22 was influenced by the lowering of the viscosity with not only the concentration of impurities in the intergranular glass but also the increase in the (Y + Al)/Si ratio, which probably corresponded to an approach to a eutectic composition in the system. The reduction in volume fraction of the intergranular phase and the grain growth generally improve the refractoriness, but actually did not affect it in DYA22.

DYA22(2-6), UYA22(2-6), DYA22(1) and DYA22(30) had higher strengths at moderate temperatures (400–800 or 1000°C), in that order (Fig. 1). It primarily depends on their fracture toughness ($\sigma = K_{IC}/(Y \cdot C^{1/2})$: σ; strength, K_{IC}; fracture toughness, C; flaw size, Y; constant). The increase of fracture toughness value was observed

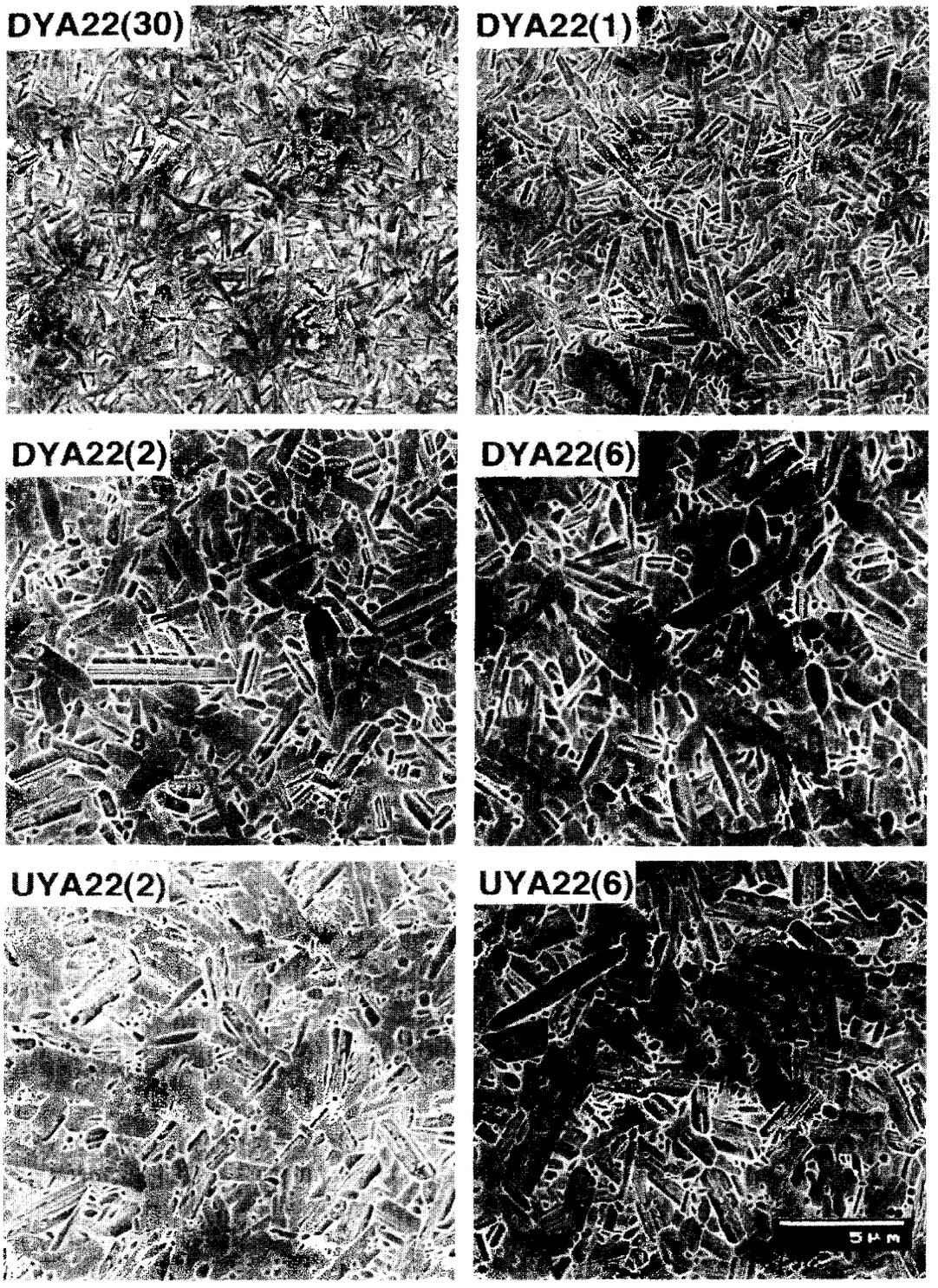

Fig. 6. Microstructure development of $Y_2O_3 + Al_2O_3$-doped Si_2N_2O ceramics. The samples were plasma-etched using an etchant gas of CF_4 before SEM observation.

in DYA22 with the hot-pressing time, as shown in Fig. 4. The fracture modes of polycrystalline ceramics are roughly divided into intergranular and transgranular fractures. The crack in DYA22 propagated more intergranularly with increasing hot-pressing time, as shown in Fig. 8. Therefore, the increase in fracture toughness probably is ascribed to grain bridging and wedging following crack deflection (i.e. intergranular fracture). The intergranular fracture of liquid-phase sintered ceramics such as the Si_2N_2O ceramics is dependent on the thermal residual stress in the vicinity of the intergranular phase. The residual stress is primarily developed by a thermal expansion mismatch between Si_2N_2O grains and the intergranular glassy phase.

Taya *et al.*[21] determined the thermal residual stresses in a spherical particulate composite using the modified Eshelby model. The average thermal stresses in the particulate (Si_2N_2O grain) $<\sigma>_p$

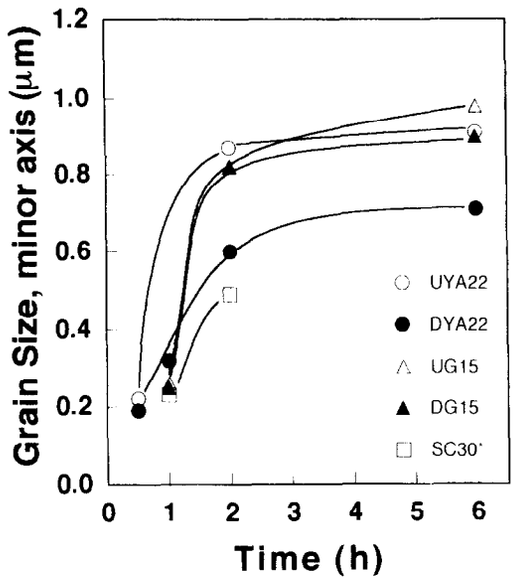

Fig. 7. Average grain size (minor axis) of elongated grains in the Si_2N_2O ceramics. (SC30*: Ref. 4).

and in the matrix (the intergranular glass) $<\sigma>_m$ are given by the following equations:

$$<\sigma>_p / E_m = -2(1-f_p)\beta(\alpha_p - \alpha_m)\Delta T/A \quad (1)$$

$$<\sigma>_m / E_m = 2f_p\beta(\alpha_p - \alpha_m)\Delta T/A \quad (2)$$

where

$$A = (1-f_p)(\beta+2)(1+\nu_m) + 3\beta f_p(1-\nu_m)$$

$$\beta = \left(\frac{1+\nu_m}{1-2\nu_p}\right)\left(\frac{E_p}{E_m}\right)$$

In order to calculate the thermal stress in the composite (the Si_2N_2O ceramics) at room temperature,

Table 3. Chemical compositions of the intergranular glassy phases in the Si_2N_2O ceramics doped with $Y_2O_3+Al_2O_3$ or Gd_2O_3. (Me*=Y or Gd)

Eq%	Me*	Al	Si
DYA22(30)	25·8	15·0	59·2
DYA22(2)	35·7	18·8	45·5
UYA22(30)	26·2	16·4	57·4
UYA22(2)	35·1	20·0	44·9
DG15(1)	44·1	—	55·9
UG15(1)	42·0	—	58·0

T_R, the composite is assumed to be subjected to a temperature change, $\Delta T = T_R - T_g$, where T_g denotes the glass transition temperature at which the stresses are no longer relaxed. E_i, ν_i and α_i are Young's modulus, Poisson's ratio and the coefficient of thermal expansion (CTE) of the ith phase, where i=m and p represent the matrix and particulate, respectively. f_p is the volume fraction of the particles.

Y–Al–Si–O–N glasses (Synthesized glasses) with compositions close to the measured compositions of the intergranular glasses were fabricated and evaluated as shown in Table 4. The synthesized glasses were nearly saturated with nitrogen. (When greater amounts of nitrogen were added into the glasses, they devitrified during cooling.) The average thermal residual stresses in the Si_2N_2O ceramics were calculated using the room-temperature properties of Si_2N_2O and the synthesized Y–Al–Si–O–N glasses. f_p were estimated from the starting composition, the composition of the intergranular phase and the specific gravities of the glasses and Si_2N_2O.

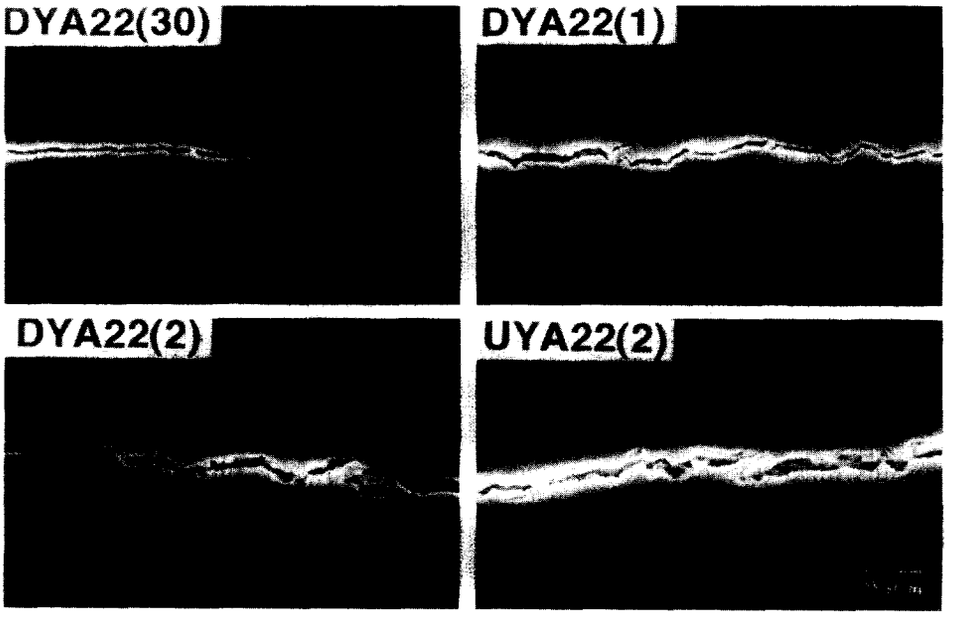

Fig. 8. Representative crack deflection profiles of the $Y_2O_3+Al_2O_3$-doped Si_2N_2O ceramics (DYA22, UYA22).

Table 4. Chemical compositions, properties (density (ρ), Young's modulus (*E*), Poisson's ratio (ν), the coefficient of thermal expansion (α) and glass transition temperature (T_g)) of synthesized oxynitride glasses and Si_2N_2O, the volume fraction of Si_2N_2O grains in the ceramics (f_p), and the average thermal residual stresses in the grains $<\sigma>_p$ and in the intergranular glassy phase $<\sigma>_m$

	Synthesized glass (eq%)					ρ	*E*		α×10^{-6}	T_g		$\langle\sigma\rangle_m$	$\langle\sigma\rangle_p$
	Me*	Al	Si	O	N	(g/cm^3)	(GPa)	ν	(°C)	(°C)	f_p	(MPa)	(MPa)
DYA22(30), UYA22(30)	26·0	18·5	55·5	80·0	20·0	3·66	137	0·28	6·9	934	0·92	374	−33
DYA22(2),UYA22(2)	36·0	19·2	44·8	75·0	25·0	4·01	146	0·29	7·1	945	0·94	440	−28
DG15(1),UG15(1)	40·0	—	60·0	80·0	20·0	5·67	136	0·26	7·7	951	0·95	467	−25
Si_2N_2O(SC30-120)[a]	—	—	—	—	—	2·81[b]	239	0·21	3·4	—	—	—	—

*Me=Yor Gd.
[a]ref. 4.
[b]The theoretical densities calculated from the lattice constants of Si_2N_2O.

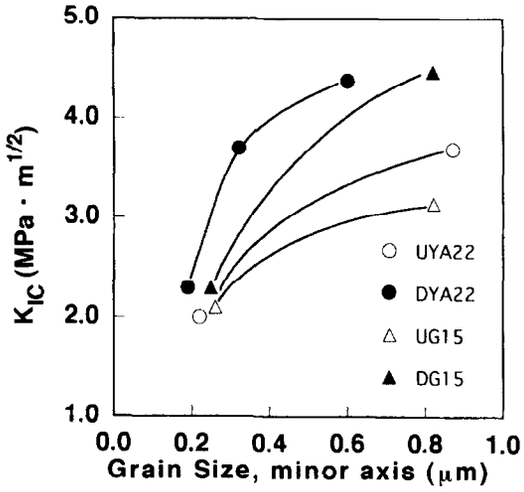

Fig. 9. Fracture toughness (K_{IC}) of the Si_2N_2O ceramics doped with $Y_2O_3+Al_2O_3$ or Gd_2O_3 as a function of grain size (minor axis).

The CTEs of the synthesized glasses are greater than that of Si_2N_2O; therefore, the average stresses in Si_2N_2O grains (particulates) $<\sigma>_p$ and the intergranular glassy phases (matrices) $<\sigma>_m$ are in compression and tension, respectively, as shown in Table 4. A high tensile stress in the intergranular phase seems to lead to the intergranular fracture; however, the difference in the calculated tensile stress in the matrix between DYA22(2) (UYA22(2)) and DYA22(30) (UYA22(30)) is not so large that the variation in fracture mode (intergranular and transgranular fracture) is ascribed to only the difference in the tensile stress. The high average tensile residual stress in the intergranular glassy phase must be one of the important factors for the intergranular fracture, but not the sufficient condition for it.

Lange[22] showed that the particle size is one of the factors that governs the criterion of crack instability. The grains in all the Si_2N_2O ceramics were not so large that microcracks occurred around the grains during cooling. Therefore, the greater residual thermal stresses were localized in the intergranular phase around the larger grains after cooling. As shown in Figs 6 and 7, the large grain growth was observed in the ceramics hot-pressed for 2 h (DYA22(2) and UYA22(2)). Figure 9 shows the relation between the average grain size and K_{IC} for DYA22 and UYA22. The fracture toughness values seem to depend on the grain size, and increase with it. The crack is expected to propagate more preferentially in the intergranular glassy phase in the higher residual tensile stress localized around the larger grain, instead of propagating through the large grain in the residual compressive stress, especially when the crack tip reaches the large elongated grain oriented to the direction with a low incident angle for the crack. As a result of this, the grain bridging following the deflection would occur effectively. The development of large grains in DYA22(2-6) (or UYA22(2-6)) is considered to be one of the factors leading to the intergranular fracture.

The model proposed by Cutler and Virkar[23] provided the fracture toughness of a particulate composite caused by periodic residual stress field as:

$$K^a_{IC} = K^0_{IC} + A_1\sigma_1(d_1)^{1/2} \quad (3)$$

where A_1 is a constant which is dependent on d_1/d_2 and is dependent on crack length, d_1 and d_2 are the particle size and the thickness of the intergranular phase, respectively, and σ_1 is the residual compressive stress in the particle. Therefore, the apparent toughness K^a_{IC} of the composite increases with the particle size even if the fracture is predominantly transgranular. In this case, the increase by the mechanism substantially is small because the average residual compressive stress in the Si_2N_2O grain is low.

Further, the effects of the concentration of impurities have to be considered. UYA22(2-6) had a slightly larger grain size than DYA22(2-6) and an intergranular phase with a basic chemical composition similar to that of DYA22(2-6). However, the fracture toughness of UYA22(2-6) is low when compared to that of DYA22(2-6). The intergranular phase of UYA22(2-6) has the low concentration of impurities because the intergranular

phase in UYA22(2-6) derived from the pure Si_3N_4 powder evidently contains smaller amounts of impurities than that in DYA22(2-6). The residual stresses possibly are enhanced in DYA22(2-6) because the CTE of the intergranular phase generally is expected to increase with the concentration of impurities, especially F. The thermal expansion of glasses is inversely related to the strength of interatomic bond of glass network. The addition of impurities (especially F) generally increases nonbridging anions and leads to a reduction in continuity of the glass network. Besides, the chemical bonding (interfacial bonding) between Si_2N_2O and the intergranular phase possibly was weakened by the concentration of impurities on the interface. These factors affected the development of intergranular fracture and the increase in fracture toughness in DYA22(2-6).

As shown in Fig. 1, the strengths of UYA22(2-6) and DYA22(2-6) were very high at room temperature, but dropped sharply at intermediate temperatures. When the specimens were annealed at 400°C before the bending test at room temperature, the room-temperature strength of UYA22(2-6) was reduced to a level comparable to the strength at 400°C. This reveals that the high strength at room temperature is ascribed to a surface compressive residual stress induced during the grinding process before the bending tests, as reported by Johnson-Walls *et al.*[24]

4.3 Gd_2O_3 addition

Elongated Si_2N_2O grains also grew with increasing the hot-pressing time from 1 to 2 h, but with no additional increase by hot-pressing for a period from 2 to 6 h in the case of Gd_2O_3 addition, as shown in Fig. 7. Impurities hardly affected the grain growth in the Gd_2O_3-doped samples. Crystallization in the intergranular phase occurred in both the samples (DG15 and UG15) hot-pressed for 2 h and more during cooling. Gd–N–apatite ($Gd_5(SiO_4)_3N$) precipitated at triple grain junctions.

The onset temperature, at which the degradation of strength started to occur, shifted toward lower temperature with increasing the hot-pressing time from 1 to 2 h (Fig. 2), as shown in the case of the $Y_2O_3 + Al_2O_3$ additions. The retention in strength at high temperatures is roughly dependent on the refractoriness (the viscosity) of the residual intergranular glassy phases in the samples. The high strength of DG15(1) at 1500°C is believed to be the result of the high refractoriness of a Gd–Si–O–N glass of the intergranular phase in it. Plastic deformation occurred slightly at 1400°C and more in the bending tests at a lower crosshead speed because of its small grain size and the relatively large amounts of the intergranular glassy phase. The strength of DG15(2-6) started to drop sharply as low as 800°C. In the previous work,[4] the temperature dependence of flexural strength of Ce-doped Si_2N_2O ceramics (SC30) prepared from the impure powder was examined, and a similar shift was observed. It was suggested that the degradation of strength in the high temperature range resulted from the intergranular crystalline phase (Ce–N–apatite) instability in air and the low softening temperature of (1) the intergranular amorphous phase produced by the decomposition of the intergranular crystalline phase, and/or (2) residual glassy films containing large concentrations of impurities which remained at grain boundaries following crystallization. In this case, Gd–N–apatite ($Gd_5(SiO_4)_3N$) is more stable in air than Ce–N–apatite, and not easily oxidized during the brief exposure at the bending tests. In addition, when the ceramics were prepared from the pure Si_3N_4 powder, the high-temperature strength was improved appreciably (see the temperature dependence of strength of UG15(2-6) in Fig. 2). Therefore, the degradation in strength of DG15(2-6) was probably caused by the low softening temperature of the residual glassy films with large concentrations of impurity elements. Moreover, with the crystallization in the intergranular phase, the composition of the residual glassy film approached to a eutectic point of the system, at which point the softening temperature is generally low. It also led to the degradation.

The fracture toughness in the Gd_2O_3-doped samples increased with increasing the hot-pressing time from 1 to 2 h as shown in the case of the $Y_2O_3 + Al_2O_3$ additions (Fig. 4). The crack in DG15(2-6) propagated along the intergranular phase, whereas it propagated transgranularly in DG15(1). The average thermal stresses in the Si_2N_2O grains $<\sigma>_p$ and in the intergranular phase $<\sigma>_m$ in DG15(1) are calculated and given in Table 4. The tensile stress in the intergranular glassy phase was greater than that of DYA22(2-6) with a relatively high fracture toughness of 4·4 $MPa \cdot m^{1/2}$; however, the fracture in DG15(1) was predominantly transgranular and the fracture toughness was low. Figure 9 shows the relation between the average grain size and K_{IC} for UG15 and DG15. The fracture toughness depended on the grain size, and increased with it in the same manner as that in the case of the $Y_2O_3 + Al_2O_3$ additions. DG15(1) had a small average grain size of 0·21 μm (minor axis) like DYA22(30). The transgranular fracture in DG15(1) seems to be the result of the small grain size of the Si_2N_2O and possibly the low

concentrations of impurities in the intergranular glass without crystallization, as can be inferred from the high strength at high temperatures.

The intergranular fracture was observed in DG15(2-6) with a higher fracture toughness value than DG15(1). It is roughly estimated that the Si_2N_2O grains in DG15(2-6) were in a more compressive stress field because the crystallization of the N–apatite with a high CTE* seemed to occur in triple grain junctions at a relatively high temperature as compared to T_gs in the intergranular glasses, whereas the average residual tensile stress in the intergranular glassy phase did not increase substantially with the crystallization because there is no appreciable difference in CTE between Gd–N–apatite* and the Gd–Si–O–N glass ($7{\cdot}7\times10^{-6}$/°C) (or the CTE of the apatite is considered to be somewhat greater than that of the glass) and the decrease in volume fraction of the glassy phase by crystallization does not affect the tensile stress so much. (*The CTE of La–N–apatite ($La_5(SiO_4)_3N$) has already been measured as 10.1×10^{-6}/°C,[25] and the CTE of Gd–N–apatite was estimated to be a little smaller than that of La–N–apatite because Gd has a relatively small ionic radius and a high cationic field strength (z/r^2: where z = valence and r = bond length) as compared to La). However, the grain in DG15 grew appreciably with the increase of the hot-pressing time from 1 to 2 h, as shown in Fig. 7. A greater thermal stress was consequently localized in the intergranular glassy phase around the larger grains in DG15(2-6) with the grain growth than in DG15(1).The effect of impurities on toughening in DG15(2-6) was also examined. The fracture toughness of UG15(2-6) prepared from the pure powder was lower than DG15(2-6) (Fig. 3) as shown in the case of the $Y_2O_3+Al_2O_3$ additions. Besides, the fracture toughness increased to the level of DG15(2-6) with 4000 ppm F doped to UG15 (see UG15F(6) in Fig. 3). They also reveal that impurities (e.g. F) are effective not only on the fracture toughness of Si_2N_2O ceramics, but on high-temperature strength. The toughening of the Gd-doped Si_2N_2O ceramics was also effected by the following three factors: (1) the thermal tensile stress in the residual glassy films and the compressive stress in the Si_2N_2O grains, (2) the large grain size, and (3) the impurities concentrated in the glassy films, in analogy with that of the $Y_2O_3+Al_2O_3$-doped ones. (Needless to say, the three factors are not independent of each other.) The difference in fracture toughness between DG15(2-6) and DG15(1) was primarily caused by factors (2) and (3).

In the previous work,[4] it was suggested that the toughening in the Ce-doped ones hot-pressed for 2 h (SC30-120) was primarily dependent on the crystallization of Ce–N–apatite with a higher CTE in the intergranular phase. However, the precipitation of the apatite phase probably affected the thermal stress in the Si_2N_2O grains, but not in the intergranular glassy films as mentioned above. The toughening in the Ce-doped ones is also considered to depend not only on the enhancement of the residual stress by the crystallization, but also the same mechanisms as that of the Gd-doped ones. (The average grain size of SC30-120 is relatively small, as shown in Fig. 7, when compared with those of UYA22(2) and DG15(2), but the toughening by crack deflection/grain bridging was observed with relatively large elongated Si_2N_2O grains in the sample (Fig. 3 in the previous article[4]).)

5 CONCLUSIONS

The high-temperature strength degradation of the Si_2N_2O ceramics was governed by the refractoriness (viscosity) of the intergranular glassy phase. The refractoriness was dependent on the basic chemical composition (the kind of additives and Me/Si ratio) of the intergranular glassy phase and impurities included in raw powders, but not seriously the grain size of Si_2N_2O and the volume fraction of the intergranular phase in the case of the bending tests in the high crosshead speed. The strength at low temperatures was primarily caused by the fracture toughness.

The toughening of the ceramics was believed to be ascribed to grain bridging and wedging following intergranular fracture. The intergranular fracture of the ceramics was affected by the following three factors: (1) the average thermal tensile stress in the intergranular glassy phase and the compressive stress in Si_2N_2O grains, primarily developed by the thermal expansion mismatch between Si_2N_2O grains and the intergranular glassy phase, (2) the higher tensile residual stress localized in the intergranular glassy phase (film) around the larger Si_2N_2O grains, and the increase in CTE of the intergranular glass, and (3) the decrease in the chemical bonding on the interface between Si_2N_2O grains and the intergranular glass with the concentration of impurities in the intergranular glassy phase.

REFERENCES

1. BILLY, M., BOCH, P., DUMAZEAU, C., GLANDUS, J. C. & GROUSAT, P., Preparation and properties of new silicon oxynitride based ceramics. *Ceram. Int.*, **7** (1981) 13–18.
2. HUANG, Z. K., GREIL, P. & PETZOW, G., Formation of silicon oxynitride from Si_3N_4 and SiO_2 in the presence of Al_2O_3. *Ceram. Int.*, **10** (1984) 14–17.

3. TRIGG, M. B. & JACK, K. H., Silicon oxynitride and o'-sialon ceramics. In *Proc. Int. Symp. on Ceramic Components for Engines*, Hakone, Japan, 1983, ed. S. Somiya, E. Kanai & K. Ando. KTK Scientific Publishers, Tokyo, Japan, 1984, pp. 199–207.
4. OHASHI, M., KANZAKI, S. & TABATA, H., Processing, mechanical properties and oxidation behaviour of silicon oxynitride ceramics. *J. Am. Ceram. Soc.*, **74** (1991) 109–14.
5. OHASHI, M., KANZAKI, S. & TABATA, H., Effect of additives on some properties of silicon oxynitride ceramics. *J. Mater. Sci.*, **26** (1991) 2608–14.
6. OHASHI, M., HIRAO, K., NAGAOKA, T., WATARI, K., YASUOKA, M., KANZAKI, S. & SHIMAMORI, T., Preparation of dense silicon oxynitride ceramics by HIPing. *Brit. Ceram. Trans. J.*, **91** (1992) 202–7.
7. OHASHI, M., KANZAKI, S. & TABATA, H., Influence of seeding on the reaction sintering of silicon oxynitride. *J. Ceram. Soc. Japan (Seramikkusu Ronbunshi)*, **97** (1989) 559–65.
8. LOEHMAN, R. E., Preparation and properties of yttrium–silicon–aluminium oxynitride glasses. *J. Am. Ceram. Soc.*, **62** (1979) 491–4.
9. DREW, R. A. L., HAMPSHIRE, S. & JACK, K. H., The preparation and properties of oxynitride glasses. In *Progress in Nitrogen Ceramics*, ed. F. L. Riley. Nijhoff, The Hague, The Netherlands, 1983, pp. 323–30.
10. HAMPSHIRE, S., DREW, R. A. L. & JACK, K. H., Viscosities, glass transition temperatures and microhardness of Y–Si–Al–O–N glasses. *J. Am. Ceram. Soc.*, **67** (1984) C46–C47.
11. OHASHI, M., NAKAMURA, K., HIRAO, K., KANZAKI, S. & HAMPSHIRE, S., Formation and properties of Ln–Si–O–N glasses (Ln = lanthanides or Y). *J. Am. Ceram. Soc.*, **78** (1995) 71–6.
12. LANGE, F. F., High-temperature strength behaviour of hot-pressed Si_3N_4: Evidence for subcritical crack growth. *J. Am. Ceram. Soc.*, **57** (1974) 84–7.
13. ISKOE, J. L., LANGE, F. F. & DIAZ, E. S., Effect of selected impurities on the high temperature mechanical properties of hot-pressed silicon nitride. *J. Mater. Sci.*, **11** (1976) 908–12.
14. CLARK, D. R., Densification of silicon nitride: Effect of chlorine impurities. *J. Am. Ceram. Soc.*, **65** (1982) C21–C23.
15. BRAUE, W., WOTTING, G. & ZIEGLER, G., Influence of impurities in different processed Si_3N_4-powders on high-temperature properties of sintered materials. *Brit. Ceram. Proc.*, **37** (1986) 71–80.
16. NAKAJIMA, Y., TSUGE, A., SANO, A., MITAMURA, R. & KANZAKI, S., Development of silicon nitride and silicon carbide powders. In *Fine Ceramics, Jisedai Kenkyu Kaihatsu no Kiseki to Seika, Engineering Research Association for High Performance Ceramics*. Tokyo, Japan, 1993, pp. 1295–1314 (in Japanese).
17. ISOZAKI, K., HIROTSURU, H., YOSHIDA, A. & SUGIMOTO, I., Influence of halogen in powder on high temperature properties of silicon nitride. In *Advanced Materials '93, I/A: Ceramics, Powders, Corrosions and Advanced Processing*, ed. Mizutani *et al. Trans. Mat. Res. Soc. Jpn, Vol. 14A*. Elsevier Science B.V., The Netherlands, 1994, pp. 565–8.
18. TANAKA, I., IGASHIRA, K., KLEEBE, H. J. & RUHLE, M., High-temperature strength of fluorine-doped silicon nitride. *J. Am. Ceram. Soc.*, **77** (1994) 275–7.
19. MARSHALL, D. B. & EVANS, A. G., Reply to comment on "Elastic/plastic indentation damage in ceramics: the median/radial crack system". *J. Am. Ceram. Soc.*, **64** (1981) C182–C183.
20. LEWIS, M. H., REED, C. J. & BUTLER, N. D., Pressureless-sintering ceramics based on the compound Si_2N_2O. *Mater. Sci. Eng.*, **71** (1985) 87–94.
21. TAYA, M., HAYASHI, S., KOBAYASHI, A. S. & YOON, H. S., Toughening of a particulate-reinforced ceramic-matrix composite by thermal residual stress. *J. Am. Ceram. Soc.*, **73** (1990) 1382–91.
22. LANGE, F. F., Criteria for crack extension and arrest in residual localized stress fields associated with second phase particles. *Fracture Mechanics of Ceramics*, **2** (1974) 599–609.
23. CUTLER, R. A. & VIRKAR, A. V., The effect of binder thickness and residual stresses on the fracture toughness of cemented carbides. *J. Mater. Sci.*, **20** (1985) 3557–73.
24. JOHNSON-WALLS, D., EVANS, A. G., MARSHALL, D. B. & JAMES, M. R., Residual stresses in machined ceramic surfaces. *J. Am. Ceram. Soc.*, **69** (1986) 44–7.
25. MITOMO, M., IZUMI, F., HORIUCHI, S. & MATSUI, Y., Phase relationships in the system Si_3N_4–SiO_2–La_2O_3. *J. Mater. Sci.*, **17** (1982) 2359–64.